ACS APPLIED MATERIALS & INTERFACES

Letter

www.acsami.org

Laser Annealing of Nanocrystalline Gold Nanowires

Jungyun Kim,[†] Chia-Yu Lin,[‡] Wendong Xing,[‡] Martha L. Mecartney,[†] Eric O. Potma,*[,‡] and Reginald M. Penner*[,†,‡]

[†]Department of Chemical Engineering and Materials Science, University of California, Irvine, California 92697-2700, United States

[‡]Department of Chemistry, University of California, Irvine, California 92697-2025, United States

ABSTRACT: The efficacy of laser annealing for the thermal annealing of nanocrystalline gold nanowires is evaluated. Continuous laser illumination at 532 nm, focused to a 0.5 μm diameter spot, was rastered perpendicular to the axis of nanocrystalline gold nanowire at ~2 kHz. This rastered beam was then scanned down the nanowire at velocities from 7 to 112 nm/s. The influence on the electrical resistance of the gold nanowire of laser power, polarization, translation speed, and nanowire width were evaluated. Nanocrystalline gold nanowires were prepared on glass surfaces using the lithographically patterned nanowire electrodeposition (LPNE) method. These nanowires had a rectangular cross section with a height of 20 ($\pm$ 3) nm and widths ranging from 76 to 274 nm. The 4-contact electrical resistance of the nanowire is measured in situ during laser annealing and a real-time decrease in electrical resistance of between 30 and 65% is observed, depending upon the laser power and scan rate along the nanowire. These resistance decreases are associated with an increase in the mean grain diameter within these nanowires, measured using transmission electron microscopy, of up to 300%. The observed decrease in the electrical resistance induced by laser annealing conforms to classical predictions based upon the reduction in grain boundary scattering induced by grain growth.

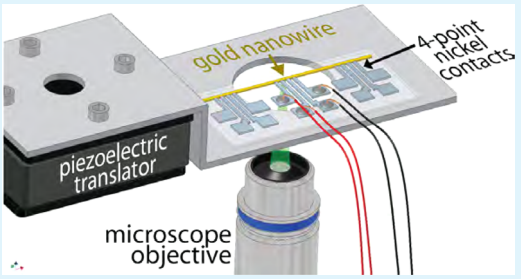

KEYWORDS: *zone, photolithography, electrodeposition, grain growth, electrical resistivity*

1. INTRODUCTION

Metal nanowires play an essential roll as electrical conduits in present day integrated circuits,[1] and metal nanowires are projected to fulfill this roll in many proposed next-generation nanometer-scale circuits.[2−5] To minimize the energy dissipated by a metal nanowire per unit time, i^2R, we must minimize its resistance, R. The value of R is proportional to the apparent resistivity of the metal, $R = (\rho_{app}l)/A$, where l is the wire length and A is the cross-sectional area of the nanowire. In this equation, ρ_{app} itself depends upon the identity of the metal, on the lateral dimensions of the nanowire, and on the mean grain diameter, d, of the metal if it is polycrystalline. As the value of d is decreased, ρ_{app} increases because electrons can be reflected from grain boundaries contributing to dissipation.[6,7] In fact, the resistance contribution of single grain boundaries has been directly measured for gold nanowires, where a value of 4−10 Ω/grain boundary was obtained.[8]

Long (l > 10 μm) metal nanowires prepared by electron beam lithography,[9,10] electrodeposition,[11,12] and many other methods[13−18] are nanocrystalline with grain diameters in the 2−50 nm range. For nanocrystalline metal nanowires with lateral dimensions that are greater than the mean grain diameter, the electrical resistance is dominated by grain boundary scattering as opposed to either surface scattering or the intrinsic resistivity of the metal.[6,7] The deleterious influence of grain boundaries on the electrical properties of mesoscopic, polycrystalline metal wires provides a strong motivation for developing postprocessing methods for increasing the mean grain diameter.

For metal nanowires that are confined to a trench, as is the case for the copper nanowires prepared using the dual Damascene method,[19] conventional thermal annealing can be used to increase the grain diameter and reduce the electrical resistance.[1,20] For metal nanowires that are patterned onto a planar surface, however, thermal annealing induces a classic Rayleigh instability,[21,22] causing the decomposition of the nanowire into a linear ensemble of hemispherical metal nanoparticles. This dramatic shape transformation occurs even for modest temperatures and short annealing times. For example, a 40 nm (w) × 20 nm (h) gold nanowire prepared by lithographically patterned nanowire electrodeposition (LPNE) that is electrically continuous for hundreds of micrometers (Figure 1a) shows multiple discontinuities after thermal annealing for just 30 min at 300 °C, even though the melting point for gold is 1064 °C (Figure 1b).

How then can grain growth be accomplished without decomposing the nanowire? In principle, grain growth requires the short-range motions of metal atoms ($d \approx 1$ nm), while mass displacements across much larger distances ($d \approx 10-100$ nm) are required to cause shape changes and the formation of nanometer-scale gaps on the scale seen in Figure 1. This

Received: May 7, 2013
Accepted: July 15, 2013
Published: July 15, 2013

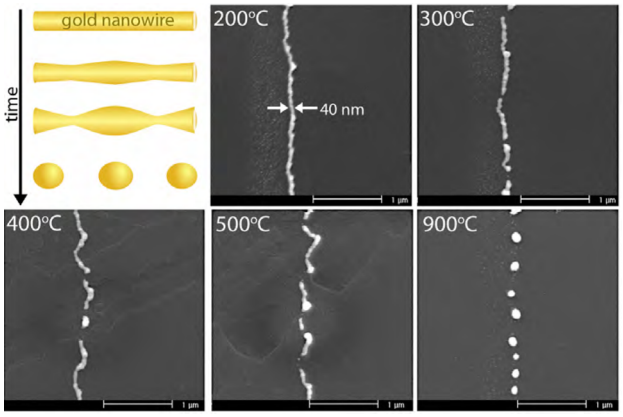

Figure 1. The Rayleigh instability, shown schematically at upper left, thwarts attempts to achieve grain growth in metal nanowires using thermal annealing.[21,22] For example, shown here are scanning electron micrographs of an ~40 nm ×20 nm gold nanowire prepared by LPNE on glass after thermal annealing in air at the indicated temperature for 30 min. Decomposition of the nanowire proceeds on this time scale producing breaks in the nanowire even at 300 °C = 0.28T_m.

disparity in length scales provides the basis for a testable hypothesis for effecting grain growth that involves rapid, highly localized, heating followed by rapid cooling of nanowire sections. Laser annealing was used to test this strategy for gold nanowires having an initial grain diameter of 27 nm prepared using our LPNE method. Here, we report in situ measurements of the 4-contact electrical resistance for single gold nanowires. The real-time electrical resistance of these nanowires during annealing is decreased by 30−65%, depending upon the laser power and scan rate along the nanowire. Transmission electron microscopy of these nanowires shows that the observed resistance decrease derive from an increase in the mean grain diameter of up to 300%.

In previous work, laser annealing has been successfully used to increase the electrical conductivity of silicon nanowires[23] and zinc oxide nanowires,[24] but the influence of laser irradiation on the grain diameters of these materials were not measured in these studies. Laser annealing was also employed to alter the saturation current and threshold voltage for single indium oxide nanowire transistors.[25] We are unaware, however, of any prior attempts to accomplish grain growth in metal nanowires using this approach.

2. EXPERIMENTAL SECTION

The experimental apparatus employed for this study (Figure 2a) provided the means for simultaneously measuring the 4-contact electrical resistance of a single nanowire during in situ laser illumination and annealing. The details of this process are described below.

Nanowire Deposition and In Situ Resistance Measurement. Nanocrystalline gold nanowires were patterned onto glass coverslips using the LPNE method as previously described.[11,12,26] These nanowires had a rectangular cross section with a height of 20 (± 3) nm and widths ranging from 76 to 274 nm. The four-probe electrical resistance on a single gold nanowire was measured using a source meter (Keithley Instruments, model 2400) in conjunction with a digital multimeter (Keithley Instruments, model 2000). Ni contacts were patterned from the evaporated Ni layer deposited in the first step of the LPNE process using a second lithography cycle (Figure 2d). Nitric acid acid was again used to etch the exposed Ni through the patterned photoresist to produce three sets of four identical pads, electrically continuous to the Au nanowire (Figure 2d, step 4). The electrically isolated length between the two center contacts was 200 μm with 40 μm separating the outermost contacts. An initial voltage bias of 5 mV was applied during the in situ resistance measurement.

Wire Illumination and Translation. Nanowires were annealed using continuous wave laser radiation at wavelengths

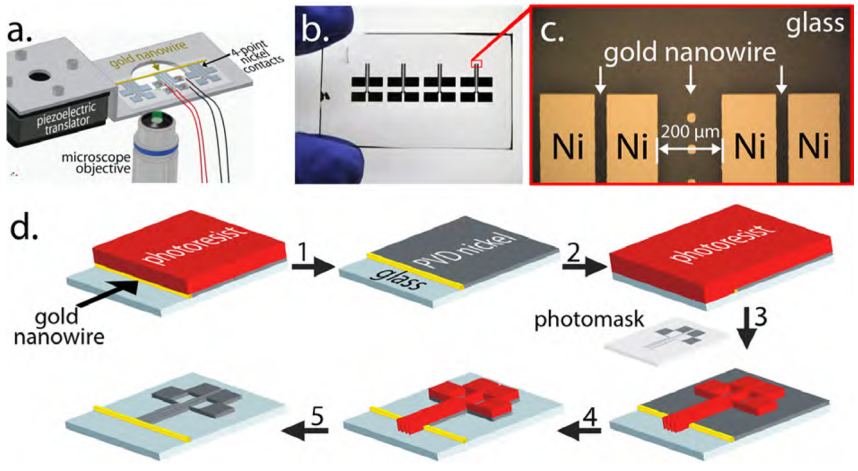

Figure 2. (a) Schematic drawing of the apparatus used for the laser annealing of nanocrystalline gold nanowires and electrical resistivity measurements. (b) Photograph of four, 4-point probes patterned in nickel on a glass slide. A single gold nanowire prepared using LPNE spans the entire horizontal length separating these four devices of more than 3 cm. (c) Photomicrograph of one 4-point probe showing the location of the nanowire, horizontally oriented in this image and in direct contact with the ends of the four nickel electrodes. The separation between the innermost two electrodes is 200 μm. (d) Process flow for the preparation by photolithography of tangential nickel electrical contacts on a single gold nanowire as shown in a−c. After the growth of a gold nanowire using LPNE, the photoresist is removed using acetone (step 1) and a new layer of photoresist is spin-coated to fully cover the nanowire/nickel film (step 2). A new photoresist layer is then photolithographically patterned using a four-probe photomask (step 3) and the exposed nickel film is removed with nitric acid (step 4). Finally, removal of the photoresist with acetone exposes the gold nanowire with four tangential nickel contacts (step 5).

dx.doi.org/10.1021/am401716u | ACS Appl. Mater. Interfaces 2013, 5, 6808−6814

of 532 and 800 nm; both of which were generated from a Nd:Vanadate laser (Verdi V5, Coherent, Mountain View). The raster of a 0.50 μm diameter TEM00 beam spot from a dry 20×, 0.75 NA objective lens (UplanSApo, Olympus) was controlled using a galvanometric scan head (Olympus Fluoview 300) interfaced to an inverted microscope (Olympus IX-71).

The excitation power at the sample was tuned in the range of 2.5 to 10 mW by an attenuator plate before entering the microscope. Polarization measurements were performed by rotating the excitation polarization from 0 to 90 degrees by means of an achromatic half-wave plate ranging from 400 to 800 nm. The length of the raster was confined to a 20 μm line centered on, and perpendicular to, the longitudinal axis of the nanowire. The scan speed of the beam was 3.95×10^4 μm/s resulting in a raster frequency of 1980 Hz. To position the nanowire segment of interest within the scan region, transmission optical images were obtained during the raster-scanning of the focused beam across the sample at a power less than 0.2 mW with detection of the transmitted light using a photomultiplier tube.

Nanowires were translated over the beam on a machined aluminum stage attached to a piezoelectric motor (NanoFlex Piezo Actuator, Thorlabs) at rates ranging from 7 to 112 nm/s with a step resolution of 7 nm. At a wire translation rate set at 28 nm/s, the annealing of a 10 μm section of the nanowire required 6 min. These raster conditions produced an integrated exposure time of the nanowire along this 10 μm segment of 1.8 s.

The absorptivity of a metal nanowire also depends upon the orientation of the electric field of the incident light relative to the long axis of the nanowires.[27] The influence of polarization on the observed annealing rate (Figure 3) reflects this disparity.

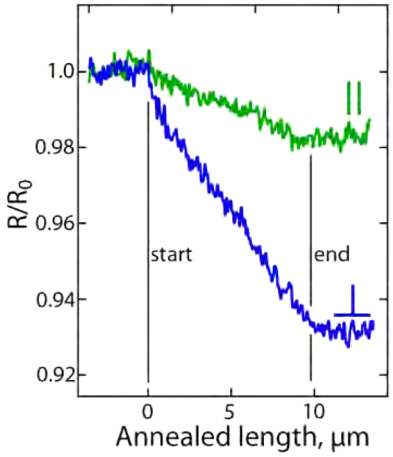

Figure 3. Influence of polarization on reduced resistance due to annealing. In situ R/R_0 versus axial laser position for the annealing of two 10 μm sections of a 20 × 276 (±14) nm gold nanowire using a linearly polarized beam (3.75 mW at 532 nm) and a translation rate of 28 nm/s. The orientation of the laser electric field relative to the wire axis is indicated, showing more rapid annealing for the perpendicular (TM) orientation. The laser raster was scanned from left to right.

Here, the wire resistance normalized to the initial resistance, R/R_0, is plotted versus the laser position along the nanowire axis. Illumination induces a reduction in R that becomes progressively larger from left to right as a longer length of the wire has been illuminated. A perpendicular orientation (TM) for the laser polarization is more efficiently absorbed.[27] λ = 532 nm TM illumination produced a 7.1% reduction in R while a parallel orientation (TE), which is more weakly absorbed, produced a reduction in R of just 1.5%. In pilot studies of the annealing process, TM illumination was associated with a greater susceptibility to wire melting than TE polarization, so for this reason TE illumination was chosen to obtain the results reported below. The wire annealing rate was also weakly dependent upon the laser wavelength (data not shown) with more rapid annealing at λ = 532 nm than at 800 nm. The origin of this disparity is stronger absorption of λ = 532 nm light by gold nanowires relative to λ = 800 nm, as previously reported. For example, for template-synthesized, cylindrical gold nanowires with diameters of 80 nm, Yao et al.[28] reported that extinction at 532 nm was higher by 16% relative to that at 800 nm. λ = 532 nm light was used for all of the other measurements reported in this paper.

Structural Characterization and Grain Size Measurement. Scanning electron micrographs of the as-processed and annealed Au wires were acquired with the ZEISS ULTRA 55 CDS ultrahigh-resolution field-emission scanning electron microscope (FE-SEM) operated at 1 keV. Before imaging, all samples were sputter-coated with an ultrathin layer (<2 nm thick) of Ir to prevent charging. Metal grains were observed and sized using the Philips CM 20 transmission electron microscope (TEM) operated at 200 keV in bright and dark field imaging modes. To maintain identical conditions for annealing of the TEM samples, TEM grids were prepared by first synthesizing Au nanowires on a glass coverslip with a thickness of 150 μm. Disks of 3 mm in diameter were cut from the coverslip with a coring device (model 350, South Bay Technology). The side of the glass without wires was then thinned by polishing to 100 μm and dimpled to produce a minimum thickness of 10 μm using an electronically dampened dimpler (500i, VCR group). Finally, an electron transparent thickness in the center of the grid was achieved by argon ion milling (1010 Ion Mill, Fischione). Nanowires were then laser-annealed in the electron transparent region.

Quantitative measurement of the average grain size was accomplished by first measuring the grain area in the plane parallel to the substrate surface. ImageJ software (http://rsbweb.nih.gov/ij/) was used to distinguish grains and grain boundaries in bright- and dark-field TEM images acquired at multiple tilt angles. The in-plane grain size, d, was defined as the diameter of a circle with an area equivalent to the measured area of the grain. For grains where the boundaries spanned the width of the wire, the average interboundary distance was measured parallel to the length of the wire.

3. RESULTS AND DISCUSSION

In situ measurements of the electrical resistance of single gold nanowires recorded during laser annealing are reported here. A diffraction-limited, 0.50 nm TEM00 laser spot at λ = 532 nm with TE polarization was rastered in the direction perpendicular to the long axis of a gold nanowire. The amplitude of this raster was 20 μm and the frequency was 1980 Hz. This raster was then scanned along the axis of the nanowire in order to effect the thermal annealing of a particular wire section while the wire resistance, R, was measured. As indicated above, nanocrystalline gold nanowires (grain dia., d ≈30 nm) were prepared by electrodeposition in conjunction with a lithographic patterning procedure (Figure 2). These nanowires had a rectangular cross-section with a height of 20 (±3) nm and widths ranging from 76 to 274 nm. The optimization of laser annealing using this

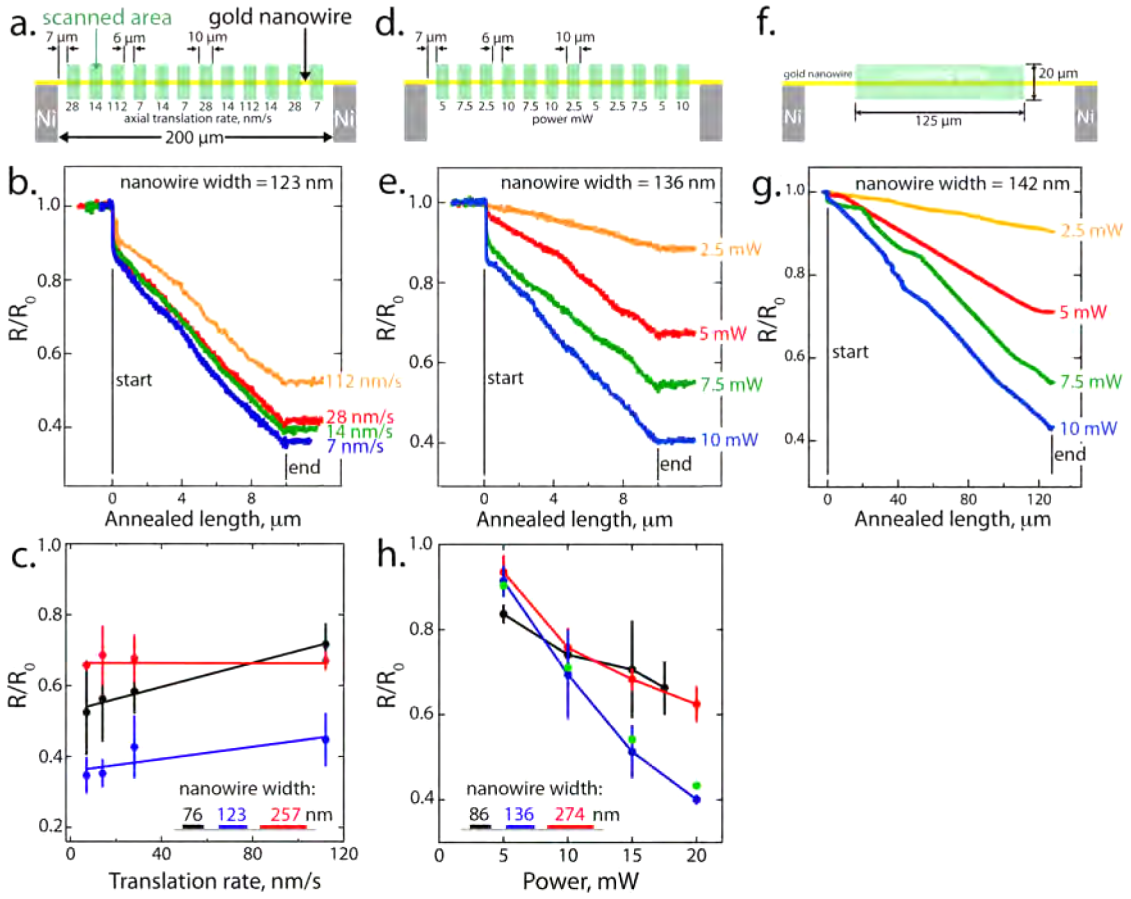

Figure 4. Laser annealing experiments probing the influence of (a–c) raster translation rate and (d–h) laser power on the measured normalized resistance change, R/R_0, for gold nanowires of three different widths as indicated. (a) Schematic diagram illustrating the experimental design for measurements of the influence of raster translation rate on R/R_0. Green rectangles represent the scanned regions. For each nanowire, 10 μm sections of the 200 μm wire length were annealed while the raster translation rate was varied as indicated, (b) R/R_0 versus annealed nanowire length data for one nanowire as a function of raster translation rate at a constant a laser power of 7.5 mW. R_0 values for the as-prepared nanowires were as follows: w = 76 nm; 43.1 kΩ, w = 123 nm; 25.4 kΩ, w = 257 nm; 2.9 kΩ. (c) Summary of R/R_0 versus raster translate rate for gold nanowires of three widths as indicated (height =20 nm). (d) Schematic diagram of the experimental design for measurements of the influence of laser power on R/R_0 at a constant 28 nm/s translate rate. For each nanowire, 10 μm sections of the 200 μm wire length were annealed while the laser power was varied as indicated. (e) R/R_0 versus annealed nanowire length data for one nanowire as a function of laser power at a constant raster translation rate of 28 nm/s. R_0 values for the as-prepared nanowires were as follows: w = 86 nm; 44.2 kΩ, w = 136 nm; 20.7 kΩ, w = 274 nm; 3.4 kΩ. (f) Schematic diagram of measurements of the influence of laser power on R/R_0 for 125 μm sections of nanowires at a constant 28 nm/s translate rate. The R_0 value for the as-prepared nanowire was: 22.7 kΩ. (g) R/R_0 versus annealed nanowire length data for 125 μm sections of four gold nanowires as a function of laser power at a constant raster translation rate of 28 nm/s/ (h) Summary of R/R_0 versus laser power for gold nanowires of three widths as indicated (height = 20 nm) and for the annealing of 125 μm wire lengths (green data points).

process requires the exploration of a large parameter space that includes laser wavelength, laser power, laser spot size, raster frequency, and raster translation rate, and all of these optimizations may be influenced by the wire dimensions.

In this initial study, we focused attention on just two of these variables: the laser power and the raster translation rate. These two variables were examined for nanowires of 20 nm height and three different widths. The influence of these two variables were examined by annealing short, 10 μm sections of nanowires as shown schematically in Figure 4 (panels a and d). Translation rates in the range from 7 to 112 nm/s and laser powers in the range from 2.5 to 10 mW were compared. Plots of the electrical resistance, R, normalized by the initial resistance, R/R_0, versus wire length data (Figure 4b,e) show a rapid drop upon the initiation illumination of the nanowire. This abrupt decrease in R/R_0 is attributed to rapid grain growth in a thermally heated region that is somewhat larger than the laser spot size. After this resistance drop, a linear decrease in R/R_0 as a function of annealed wire length is observed. The slope of this plot permits an estimation of the wire length subjected to initial heating resulting in grain growth, and this dimension is between 0.5 and 2 μm depending upon the laser power. These data support the conclusion that grain growth resulting from laser heating in this experiment is localized on the 1–2 μm length scale.

Figure 4 also shows that laser power has a much stronger influence on R/R_0 than the wire translation rate over the ranges of these two variables explored here. Specifically, R/R_0 increased only slightly (width, w = 76 or 123 nm) or not at all (w = 257 nm) when the translate rate was increased by a factor of 8 from 14 to 112 nm/s at a constant laser power of 7.5 mW (Figure 4c). In contrast, increasing the laser power from 5 to 20 mW caused a reduction in R/R_0 by one-half, on average, for nanowires ranging in width from 86 to 274 nm at a constant translation rate of 28 nm/s (Figure 4h). Wire width did not influence R/R_0 over the narrow range explored here; the wire-to-wire variability seen in panels c and h in Figure 4 are

dx.doi.org/10.1021/am401716u | ACS Appl. Mater. Interfaces 2013, 5, 6808–6814

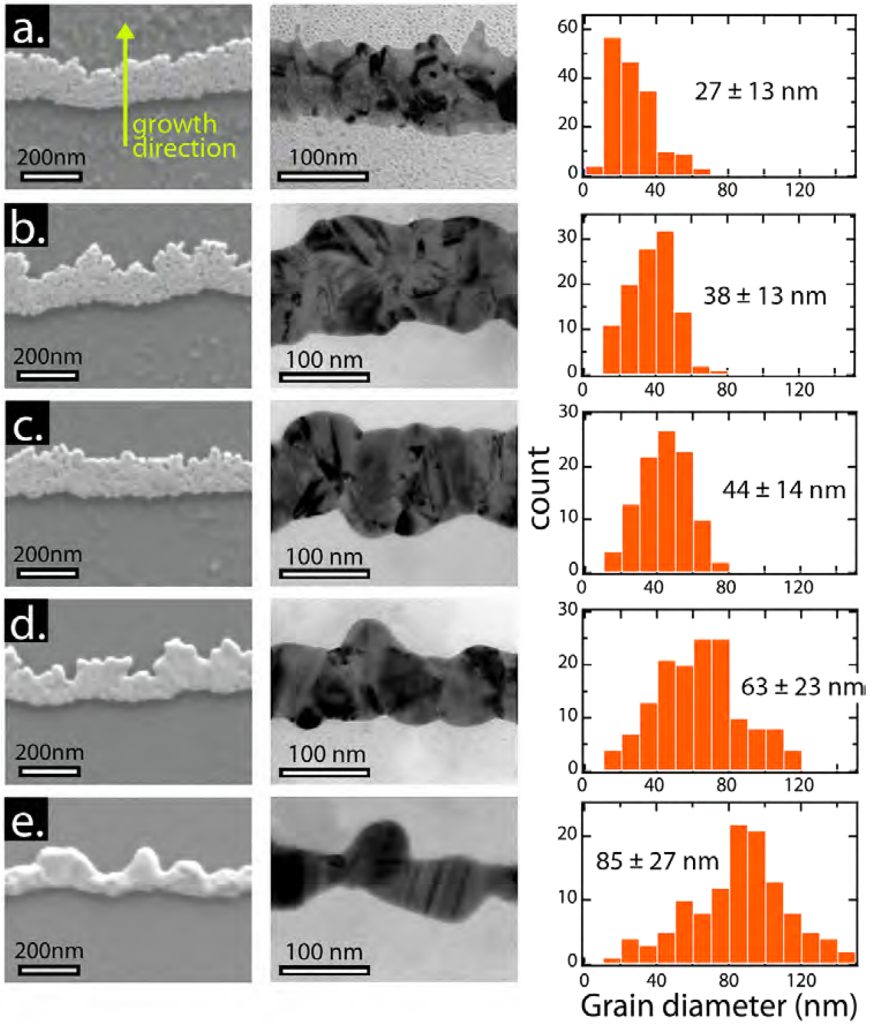

Figure 5. Electron microscopy analysis of laser annealed gold nanowires as a function of the laser power. At left is an SEM image of the nanowire (left, note that the electrodeposition growth direction is noted in a), a TEM image is shown at center, and the grain diameter histogram compiled from multiple TEM images is shown at right. The laser powers were: (a) unannealed, (b) 2.5 mW, (c) 5 mW, (d) 7.5 mW, and (e) 10 mW (SEM), 8.75 mW (TEM). The raster translation rate for all measurements was 28 nm/s.

reflective of the sample-to-sample reproducibility of these measurements. Attempts to investigate laser powers higher than 10 mW were made, but the electrical continuity of gold nanowires was usually destroyed by the formation of breaks at these higher laser fluences.

The data in panels b, c, e, and h in Figure 4 were acquired by annealing 10 μm wire lengths, but 125 μm wire lengths were also annealed (Figure 4f,g) to prove the effectiveness of laser annealing over larger length scales. The green circles in Figure 4h are the measured final R/R_0 values for 125 μm nanowire sections, where the nanowire dimensions were 20 × 142 (± 19) nm. Within our experimental error, the reduction in R/R_0 for longer wire sections is similar to that seen for the 10 μm wire lengths (Figure 4h).

The influence of laser annealing on the nanowire shape and internal grain structure was investigated using scanning electron microscopy (SEM, left-most images in Figure 5) and transmission electron microscopy (TEM, middle images in Figure 5). TEM image data permitted histograms of the grain diameter to be compiled (Figure 5, right column). For SEM analysis, a nanowire of width 130 (± 21) nm was imaged but a somewhat narrower nanowire of 80 (± 8) nm was investigated in these TEM images experiments. Both nanowires were 20 nm in height. As-prepared gold nanowires (Figure 5a) had a rough surface morphology characterized by very fine pits that were ~1−3 nm in diameter. The roughness of the solution-wetted wire edge was also rougher than the wire edge in contact with the nickel electrode (Figure 2d), a characteristic of nanowires electrodeposited using the LPNE process.[11,12,26] The mean grain diameter in this nanowire was 27 (± 13) nm. The same nanowire seen in Figure 5a is shown again after annealing at 2.5, 5, 7.5, and 10 mW (Figure 5b−e, left) using a constant translation rate of 28 nm/s. Annealing at 2.5 mW produces little observable change in the nanowire morphology, but TEM detects a slight increase in the mean grain diameter from 27 to 38 nm. At higher laser powers up to 10 mW, both the external and the internal structure of the nanowire are altered with smoothing of wire surfaces and grain growth proceeding in parallel. At a laser power of 8.75 mW, grain boundaries traverse the entire width of the nanowire producing a bamboo structure characterized by a mean grain diameter of 85 (±27) nm, a factor of 3 larger than the grain diameter of the as-prepared nanowire. Although laser annealing eliminates surface roughness of the wire, wire edges become progressively rougher with

dx.doi.org/10.1021/am401716u | ACS Appl. Mater. Interfaces 2013, 5, 6808−6814

increasing laser power, and significant constrictions are observed after treating the nanowire at 8.75 or 10 mW (Figure 5e). In parallel with this smoothing of the wire surface, the cross-section of the nanowire transitions from rectangular to semi circular. It is also apparent that at laser powers just above 10 mW discontinuities are produced in the nanowire. For example, exposure of the nanowire shown in Figure 5 to 12.5 mW light under the same conditions produced multiple breaks.

It is useful to ask whether the observed reduction in wire resistance (Figure 4) can be quantitatively attributed to the grain growth documented by TEM (Figure 5). To address this question, the electrical resistivity of a 20 × 90 nm nanowire was calculated using equations derived by Steinhögl et al.,[6,7] who treated copper nanowires having a rectangular cross section. In this case, the resistivity of a nanowire, ρ, is given by the following equation[6,7]

$$\rho = \rho_0 \left\{ 1/3 \left[\frac{1}{3} - \frac{\alpha}{2} + \alpha^2 - \alpha^3 \ln\left(1 + \frac{1}{\alpha}\right) \right] + \frac{3}{8}(1-p)\left(\frac{1}{w} + \frac{1}{h}\right)\lambda \right\} \quad (1a)$$

$$\alpha = \frac{\lambda}{d}\frac{R}{1-R} \quad (1b)$$

where ρ_0 is the resistivity of bulk gold ($\rho_{0,Au}$ = 2.27 $\mu\Omega$ cm at T = 300 K[29]), λ is the electron mean free path (40 nm), p is the specularity parameter from Fuchs-Sondheimer theory,[30,31] R is the reflection coefficient from Mayadas−Schatzkes theory,[32,33] h and w are the wire height and width, respectively, and d is the mean grain diameter.[6,7] We have previously measured the parameters p and R for gold nanowires prepared using our LPNE process and obtained values of p_{Au} = 0.379 and R_{Au} = 0.85.[12] The values of h and w employed in our calculation were 20 and 90 nm, respectively, which approximate the average values of the gold nanowires used in these measurements.

A plot of ρ versus mean grain diameter, d (Figure 6, green trace), shows that a dramatic decrease in wire resisitivity is seen as the mean grain diameter is increased across the range of grain diameters encountered in our experiments. Grain boundary (gb) scattering, in fact, is responsible for most of the electrical resistivity for these nanowires with surface scattering (s) and bulk resistivity (b) combined (red trace), accounting for a much smaller fraction of the wire resistivity. In Figure 6, experimentally measured values of ρ and d are plotted as data points with error bars that represent ±1 standard deviation for these two parameters. It is apparent that the Steinhögl equation fully accounts for the influence of d on ρ within the error of our measurements.

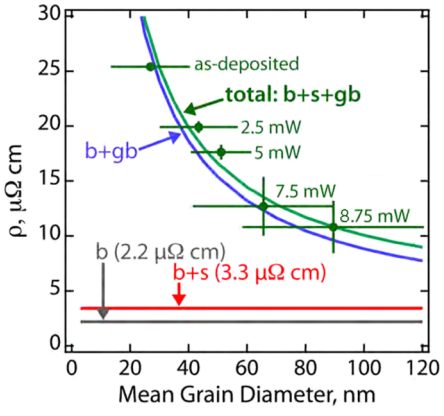

Figure 6. Calculated resistivity, ρ, vs the mean grain diameter for a 20 nm × 90 nm rectangular gold nanowire. The individual contributions of the bulk resistivity (b, gray), bulk + surface scattering resistivity (b + s, red), and bulk + grain boundary resistivity (b + gb, blue) are indicated. The experimental measurements of ρ and grain diameters measured from TEM images are plotted in green data points with error bars that represent ±1.0 standard deviation (N = 3).

4. SUMMARY

We have demonstrated that polycrystalline gold nanowires may be efficiently annealed using rastered (~2 kHz) visible laser light. Laser heating induces grain growth and an increase in the mean grain diameter by up to a factor of 3 from 27 to 85 nm. Commensurate with grain growth is a real-time reduction in the electrical resistance of the nanowire by up to 60% that occurs in quantitative agreement with the predictions of Fuchs-Sondheimer and Mayadas−Schatzkes theories. The translation rate of the nanowire under a rastering laser spot has little influence over the annealing rate, but annealing is accelerated by as much as a factor of 5 by increases in the laser power over the range from 2.5 to 10 mW. At the highest laser powers examined in this study of 10 mW, laser annealing does induce significant shape changes in the nanowire and a degradation in the width uniformity along the axis of the nanowire.

AUTHOR INFORMATION

Corresponding Author

*E-mail: rmpenner@uci.edu.

Notes

The authors declare no competing financial interest.

ACKNOWLEDGMENTS

The authors gratefully acknowledge the financial support of this work by the National Science Foundation through grant CHE-1306928. Electron microscopy was carried out in the Laboratory for Electron and X-ray Instrumentation (LEXI) at the University of California, Irvine.

REFERENCES

(1) Rosenberg, R.; Edelstein, D.; Hu, C.; Rodbell, K. *Ann. Rev. Mater. Sci.* **2000**, *30*, 229−262.
(2) Zhong, Z.; Wang, D.; Cui, Y.; Bockrath, M. W.; Lieber, C. M. *Science* **2003**, *302*, 1377−1379.
(3) Snider, G. S.; Williams, R. S. *Nanotechnology* **2007**, *18*, 035204.
(4) Xia, Q.; Robinett, W.; Cumbie, M. W.; Banerjee, N.; Cardinali, T. J.; Yang, J. J.; Wu, W.; Li, X.; Tong, W. M.; Strukov, D. B. *Nano Lett.* **2009**, *9*, 3640−3645.
(5) Jo, S. H.; Chang, T.; Ebong, I.; Bhadviya, B. B.; Mazumder, P.; Lu, W. *Nano Lett.* **2010**, *10*, 1297−1301.
(6) Steinhögl, W.; Schindler, G.; Steinlesberger, G.; Engelhardt, M. *Phys. Rev. B* **2002**, *66*, No. 075414.
(7) Steinhögl, W.; Schindler, G.; Steinlesberger, G.; Traving, M.; Engelhardt, M. *J. Appl. Phys.* **2005**, *97*, No. 023706.
(8) Bietsch, A.; Michel, B. *Appl. Phys. Lett.* **2002**, *80*, 3346−3348.
(9) Contreras, A.; Grunes, J.; Yan, X.; Liddle, A.; Somorjai, G. *Catal. Lett.* **2005**, *100*, 115−124.
(10) Jeon, K.; Lee, J.; Lee, E.; Lee, W. *Nanotechnology* **2009**, *20*, 135502.
(11) Menke, E.; Thompson, M.; Xiang, C.; Yang, L.; Penner, R. *Nat Mat* **2006**, *5*, 914−919.
(12) Xiang, C.; Kung, S.; Taggart, D.; Yang, F.; Thompson, M.; Guell, A.; Yang, Y.; Penner, R. *ACS Nano* **2008**, *2*, 1939−1949.

(13) Melosh, N.; Boukai, A.; Diana, F.; Gerardot, B.; Badolato, A.; Petroff, P.; Heath, J. *Science* **2003**, *300*, 112−115.
(14) Heath, J. *Acc. Chem. Res.* **2008**, *41*, 1609−1617.
(15) Natelson, D.; Willett, R.; West, K.; Pfeiffer, L. *Appl. Phys. Lett.* **2000**, *77*, 1991−1993.
(16) Natelson, D.; Willett, R.; West, K.; Pfeiffer, L. *Phys. Rev. Lett.* **2001**, *86*, 1821−1824.
(17) Ji, R.; Lee, W.; Scholz, R.; Gösele, U.; Nielsch, K. *Adv. Mater.* **2006**, *18*, 2593−2596.
(18) Mårtensson, T.; Carlberg, P.; Borgström, M.; Montelius, L.; Seifert, W.; Samuelson, L. *Nano Lett* **2004**, *4*, 699−702.
(19) Kaanta, C.; Bombardier, S.; Cote, W.; Hill, W.; Kerszykowski, G.; Landis, H. *Dual Damascene: a ULSI Wiring Technology* **1991**, 144−152.
(20) Ryu, C.; Kwon, K.; Loke, A.; Lee, H.; Nogami, T.; Dubin, V.; Kavari, R.; Ray, G.; Wong, S. *IEEE Trans. Electron Devices* **1999**, *46*, 1113−1120.
(21) Toimil Molares, M.; Balogh, A.; Cornelius, T.; Neumann, R.; Trautmann, C. *Appl. Phys. Lett.* **2004**, *85*, 5337−5339.
(22) Karim, S.; Toimil-Molares, M.; Balogh, A.; Ensinger, W.; Cornelius, T.; Khan, E.; Neumann, R. *Nanotechnology* **2006**, *17*, 5954−5959.
(23) Misra, N.; Xu, L.; Pan, Y.; Cheung, N.; Grigoropoulos, C. *Appl. Phys. Lett.* **2007**, *90*, 111111−111111−3.
(24) Maeng, J.; Heo, S.; Jo, G.; Choe, M.; Kim, S.; Hwang, H.; Lee, T. *Nanotechnology* **2009**, *20*, 095203.
(25) Lee, C.; Srisungsitthisunti, P.; Park, S.; Kim, S.; Xu, X.; Roy, K.; Janes, D.; Zhou, C.; Ju, S.; Qi, M. *ACS Nano* **2011**, *5*, 1095−1101.
(26) Xiang, C.; Yang, Y.; Penner, R. *Chem. Commun.* **2009**, 859−873.
(27) Zhang, X.; Liu, H.; Tian, J.; Song, Y.; Wang, L.; Song, J.; Zhang, G. *Nanotechnology* **2008**, *19*, 285202.
(28) Yao, H.; Duan, J.; Mo, D.; Yusuf Gunel, H.; Chen, Y.; Liu, J.; Schapers, T. *J. Appl. Phys.* **2011**, *110*, 094301−094301.
(29) *CRC Handbook of Chemistry and Physics*; Chapman and Hall/CRCnetBASE: Boca Raton, FL, 1999.
(30) Fuchs, K. *Proc. Cambridge Philos. Soc.* **1938**, *34*, 100−108.
(31) Sondheimer, E. *Adv. Phys.* **1952**, *1*, 1−42.
(32) Mayadas, A.; Shatzkes, M.; Janak, J. *Appl. Phys. Lett.* **1969**, *14*, 345−347.
(33) Mayadas, A.; Shatzkes, M. *Phys. Rev. B* **1970**, *1*, 1382−1389.